Hindawi
Advances in Civil Engineering
Volume 2023, Article ID 8404335, 18 pages
https://doi.org/10.1155/2023/8404335

Research Article

Study on Interfacial Interaction of Cement-Based Nanocomposite by Molecular Dynamic Analysis and an RVE Approach

A. K. Roopa,[1] **A. M. Hunashyal**,[1] **Arun Y. Patil**,[2] **Abhishek Kamadollishettar**,[1] **Bharatkumar Patil**,[1] **Manzoore Elahi M. Soudagar**,[3,4] **Kiran Shahapurkar**,[5] **T. M. Yunus Khan**,[6] **and M. A. Kalam**[7]

[1]*School of Civil Engineering, KLE Technological University, Hubballi 580031, India*
[2]*School of Mechanical Engineering, KLE Technological University, Hubballi 580031, India*
[3]*Institute of Sustainable Energy, Universiti Tenaga Nasional, Jalan IKRAM-UNITEN, 43000 Kajang, Selangor, Malaysia*
[4]*University Centre for Research and Development, Department of Mechanical Engineering, Chandigarh University, Gharuan, Punjab, Mohali, India*
[5]*Department of Mechanical Engineering, School of Mechanical, Chemical and Materials Engineering, Adama Science and Technology University, Adama 1888, Ethiopia*
[6]*Department of Mechanical Engineering, College of Engineering, King Khalid University, Abha 61421, Saudi Arabia*
[7]*School of Civil and Environmental Engineering, FEIT, University of Technology Sydney, NSW 2007, Ultimo, Australia*

Correspondence should be addressed to Arun Y. Patil; patilarun7@gmail.com and Kiran Shahapurkar; kiranhs1588@astu.edu.et

Received 25 February 2023; Revised 27 May 2023; Accepted 7 June 2023; Published 21 June 2023

Academic Editor: Junqing Zuo

There is an increased demand for cement nanocomposites in the twenty-first century due to their composition, higher strength, high efficiency, and multiscale nature. As carbon nanotubes (CNTs) possess extremely high strength, resilience, and stiffness, inclusion of carbon nanotubes in small quantities to the concrete mix makes them a multifunctional material. A molecular level understanding is significant to capacitate the macrolevel properties of these composites. In the proposed work, molecular dynamics (MD) simulations are used to understand the behaviour of the composites at the atomic level and continuum mechanics with representative volume element (RVE) homogenization modelling is carried out for interfacial interaction study of composites. The mechanical properties such as Young's modulus, shear modulus, and poisons are evaluated using previous methods of simulations for different compositions of nanomaterials in cement matrix. The FORCITE module of MD simulation and square RVE model is used to determine the mechanical, electrical properties, and elastic constants of the cement nanocomposite. The MD simulation describes the linking effect of CNT into cement matric, and the RVE modelling study reveals the pull-out effect of CNT from matrix. From experimental and analytical studies, it is found that increase in CNT till 0.5% weight fraction increases the mechanical properties about 12% and further increasing of CNT weight fraction causes a reduction in mechanical properties about 5% due to the agglomeration of nanotubes. The density of states method in MD simulation indicates that mobility of the electrons increases with an increase in carbon nanotube proportion in the composites. The experimental test results substantiate the analytical studies, and the error obtained from both approaches is less than 20%. From the analytical study, the average maximum Young's modulus, shear modulus, and bulk modulus are obtained as 46 GPa, 31 GPa, and 32 GPa for 0.5% weight fraction of CNT in cement matrix. Hence, it is concluded that 0.5% weight fraction of CNT is considered as optimum dosage to obtain better electrical and mechanical properties.

1. Introduction

Composites have a variety of applications in the construction industry. A cement composite is a major construction element. From the recent decades, a study has been carried out to make concrete stiff, strong, and conductive by the addition of carbon nanotubes. The robust strength of carbon nanotubes, their small size, and conducting property attract the researchers to develop a composite material. CNTs are an excellent reinforcement for the mechanical improvement of hardened cementitious materials via pores-filling and cracks-bridging because pores and cracks, ranging from nanoscale to microscale, frequently exist in hardened cementitious materials. The properties of cement matrix, such as stiffness, tensile strength, compressive strength, conductance, and functional properties, might be greatly enhanced by the use of CNTs [1–5].

Currently, most experimental works carried out on influence of geometrical characteristics, aspect ratio, and concentration of CNT in cementitious materials enhanced mechanical properties of the cementitious materials through crack-bridging and pore structure modification [6–8]. The understanding of composite behaviour at the atomic level is very important for analyzing the mechanical and electrical properties. The macrolevel interaction of CSH gel with carbon nanotubes is evaluated by studying the atomic level interaction. The molecular dynamics technique has recently been used in various investigations on the mechanical characteristics and atomic structure of CNT-reinforced C-S-H [9–11]. The first-age qualities of cement and concrete are controlled by tricalcium silicate (alite: C3S), which defines the early-age features [12]. During this time, alite hydration results in the formation of calcium-silicate-hydrate gel [13]. CSH gel is responsible for most of the mechanical and physical properties of cement-based products. The tobermorite 14 A°, indicates large interlayer distance which makes the Coulombic interlayer interactions relatively insignificant compared with the ionocovalent intralayer interactions, while decreasing the interlayer distance to 11 A° influences the elastic properties of composites due to the existence of water molecules as well as Ca ions. [14]. The addition of carbon nanotubes to cement proves to be promising in improving the strength of cement and modifying it as a multifunctional material. According to the findings, CNT may effectively bridge two sides of a crack and boost the composite system's tensile strength [15]. There is no discernible difference between the compressive behaviour of CNT-reinforced C-S-H and regular C-S-H due to the local-shell buckling mode dominating for the CNT in the compressive behaviour. Young's modulus and Poisson's ratio of CNT/epoxy composite obtained from the experimental tests was 2.8 GPa and 0.34, and from MD simulation, they are found to be 3.34 GPa and 0.36, respectively, for random CNT distribution with volumetric content of 2 : 5% in the matrix [16]. Hence, molecular dynamic analysis proves to be an effective method to investigate the mechanical behaviour and characteristics of cement composites, as well as other applications such as carbon-based nanomaterials, polymer-cement nanocomposites, and chemical treatments for the alteration of material properties [17].

Similarly, representative volume element (RVE) modelling is the one of the most crucial techniques required to analyze and study the smaller scale (micro or nano) materials, mechanical properties, and surface interactions. Square RVEs are preferred for estimating the effective material constants, which were found to be quite accurate in estimating the effective Young's moduli in the CNT axial direction for both long and short CNT cases [17–19]. The rate of rising in stiffness of CNT cement composite is notable only up to a certain percentage of CNT, beyond which it slows down [17]. Young's modulus of epoxy resin nanocomposite has the thickness of 25 nm if it is found to be between 0.523 and 2.16 GPa, and it is observed that regardless of the volume of fraction, the relative distribution of CNTs in the matrix had no significant effect on Young's modulus on reinforced composite [18]. The studies revealed that nanocomposites reinforced with aligned nanotubes had a higher longitudinal modulus than those reinforced with tilted nanotubes [19].

The main objective of the present study involves determining the effect of various concentrations of CNT in a cement matrix and its behaviour on interfacial interaction influencing the mechanical and electrical properties. The experimental work and microstructural analysis are carried out to know the behaviour of CNTs into the cement matrix. Furthermore, molecular dynamic simulation to understand the atomic interactions between cement and the carbon nanotube, a prototype of the composite is modelled and analyzed using material studio software. The RVE model is used to study the pull out of CNT from the matrix affecting mechanical properties. From both the previously mentioned analytical techniques, elastic constants such as Young's modulus, shear modulus, bulk modules, and Poisson's ratio are determined. The result reveals that the concentration of SWCNT influences the mechanical and electrical properties.

2. Experimental Methods

2.1. Materials. The ordinary Portland cement 43 grade is used as the matrix. Single wall carbon nanotubes (SWCNTs) are used for reinforcement. SWCNTs are obtained from Sigma-Aldrich.co USA having 2 μ diameters and containing carbon content approximately 90%. River sand of grain size less than 1.18 mm is used to prepare cement mortar paste.

2.2. Methodology. Cement nanocomposites are prepared by adding SWCNT to the cement mortar of ratio 1 : 1 with water cement ratio as 0.45. Since SWCNTs are subjected to Van der Waals repulsive forces, hence the dispersion has been carried out to ensure the homogenous mix into the cement paste. Ethanol was utilized for prescattering of SWCNT for proper blending into water, and later on, the entire mix is sonicated with the help of a probe sonicator for about 15 minutes. The sonicated SWCNT having concentrations of 0.25%, 0.5%, 0.75%, 1.0%, and 1.25% by weight of cement was added to the cement matrix as described in Table 1. The specimen size

of 20 mm × 20 mm × 80 mm as per ASTM C293 prepared for the electromechanical test to evaluate the mechanical and electrical properties of composites. After 28 days of curing, a three point load test was carried out by load cell frame of maximum capacity 10 kN at a strain rate of 1 mm/min on composites as shown in Figure 1. Microstructural analysis SEM was conducted to know the effect of SWCNT on morphology of the cement composite.

As per the experimental test, flexural strength is calculated as shown in Figure 2. It is observed that flexural strength is maximum for CSH-CNT-2 composite compared to others. The flexural strength is found to be 32.5 MPa for CHS-CNT-2 composite. SEM results indicate the dense formation of SWCNT in cement matrix which will fill up the cement pores and act as a bridge to increase the load carrying capacity of the composite. The addition of nanomaterials also arrests the formation of cracks and reduces the shrinkage of cracks [3, 20]. But the increase of SWCNT concentration leads to agglomeration in the cement matrix at certain places as shown in red color in Figure 3, which will reduce the load capacity and lead to decrease in flexural strength. As SWCNT is subjected to repulsive Van der Waals forces which cause agglomeration in the cement matrix, therefore higher concentration of CNT reduces the flexural strength. Therefore, a molecular dynamics simulation is carried out to understand the atomic level interaction and to evaluate the other mechanical properties of composites as explained in Section 3.

3. Molecular Dynamic Analysis

Molecular dynamics (MD) can be defined as the analysis of the dynamics of a system that results from allowing atoms and molecules to interact with each other for a period of time. Since C-S-H gel is the main component of cement paste and responsible for strength, hence in the present study, calcium silicate hydrate (3Cao $2SiO_2.3H_20$) and CNTs are modelled using the material studio, and MD simulations have been carried out. The mechanical properties are calculated for Young's modulus, Poisson's ratio, bulk modulus, and shear modulus in x, y, and z-directions that ascertain the interaction among CSH-CNTs.

3.1. Modelling of Calcium Silicate Hydrate and Single-Walled Carbon Nanotube. Tobermorite is a monoclinic structure that is used to model calcium silicate hydrate (CSH) gel by creating amorphous cell module using material studio software as shown in Figures 4(a) and 4(b) for different compositions of CSH and CNT as described in Table 2. For all compositions, the C-S-H structure has a calcium-to-silicon (Ca/Si) ratio of 0.83 and an equal number of silicon atoms and water molecules with a comparable single silicon chain skeleton. The lattice length is considered as 40 Å in all three mutual perpendicular directions. The angle parameters between the lattice are considered as $\alpha = \beta = \gamma = 90^{\circ}$ and primal-centre as (0, 0, 0). The carbon nanotube is modelled considering as SWCNT of space group P1 [1] along the z-axis assigning coordinates (20, 20, 20 Å) with nonperiodic

Table 1: Various concentrations of cement nanocomposite.

Composite designation	Composition
CSH-CNT-1	99.75% CSH + 0.25% CNT
CSH-CNT-2	99.50% CSH + 0.50% CNT
CSH-CNT-3	99.25% CSH + 0.75% CNT
CSH-CNT-4	99.00% CSH + 0.25% CNT
CSH-CNT-5	99.75% CSH + 1.25% CNT

structure and chiral vector as $N = 12$ and $M = 6$, with a bond length of 1.42 Å. Three number of CNT is assumed as uniform distribution of CNT in CSH gel to attain the density of 0.5 g/cc to know the interaction of these molecules and atoms. Initially, a good position of these two molecular is verified in the absence of hydrogen bonds and equilibrium condition is attained by creation of hole in amorphous cell in the vacuum space between CNT and C-S-H gel. The spacing between the CNT is taken as 13 nm and adjacent side of amorphous as 2 nm along the lattice length. Furthermore, the CSH amorphous cell is made as an initial structure which is superimposed by the CNT structure as shown in Figure 5. The weight fraction could be controlled with the loading number of molecules. However, the packing operation is permitted when the cells are empty. The density of CSH gel is taken as 1.44 g/cc [21], and energy minimization has to be performed by ramping up the density from 0.6 g/cm^3. The medium-quality energy state of the output model was set. The distribution of the CSH is taken as random with constant pressure and temperature conditions. The computation results files will include detailed information for each parameter, such as the number of molecular chains packaged into the cell and its ultimate energy value.

3.2. Molecular Dynamics Analysis. A molecular dynamic analysis needs to be performed to understand the atom level interaction to determine the mechanical and electrical properties. It is possible to do a molecular dynamics simulation if the structure is first optimized for energy which followed by geometric optimization [22]. The molecular dynamics study is performed using the FORCITE module in the material studio. The FORCITE module allows geometrical optimization and finite temperature molecular dynamics with implicit symmetry and geometry constraints. The mechanical properties are based on the classical model in molecular dynamics; a set of "Newtonian equations of motion" is used to approximate all the molecules' locations as well as their velocity, acceleration, and rotation [23, 24].

$$\frac{dE}{dR} = m\,\frac{d^2R}{dt^2}, \tag{1}$$

where E is the potential energy; R is the co-ordinates of the atoms; and m is the mass of atoms.

The geometrical optimization is used to optimize the CSH-CNT composite because if structures are not optimized before running MD simulations, the results will be erroneous. To calculate the true density of a composite, molecular dynamics calculations are required. The system's cell density progressively increases over a period of external

(a) (b)

Figure 1: Experimental work. (a) Sonicated CNT. (b) Three point loading flexural test.

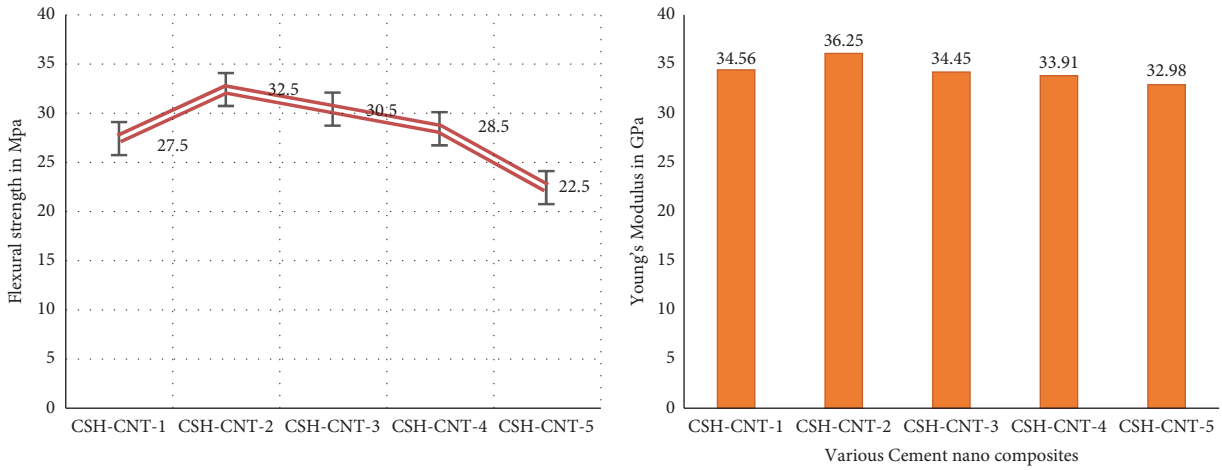

(a) (b)

Figure 2: Mechanical properties of various cement nanocomposites. (a) Flexural strength. (b) Young's modulus.

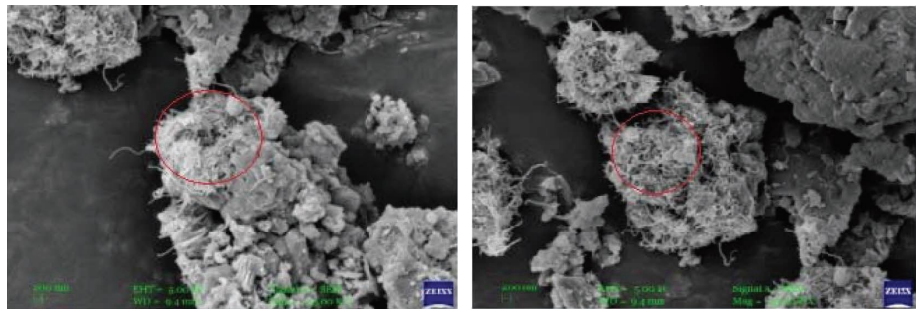

Figure 3: SEM image of the CSH-CNT composite.

pressure, and it can be further compressed by raising the pressure. From the FORCITE module, geometry optimization is selected to optimize the CSH-CNT composite by selecting a smart algorithm with NTP and default simulation time [25].

MD simulations were performed using materials studio software. The analysis was performed using the COMPASS force field. COMPASS is the first force field parameterized and validated using condensed-phase properties in addition to empirical data for isolated molecules [26, 27]. To anticipate precisely and simultaneously many molecules in isolated or condensed phases, this force field is used. The COMPASS force field consists of terms for bonds (E_b), angles (E_θ), dihedrals (E_ϕ), out-of-plane angles (χ), as well as cross-terms, and two nonbonded functions, a Coulombic function for electrostatic interactions, and a 9–6 Lennard–Jones potential for van der Waals interactions. Energy due to interaction between bond sterching bond

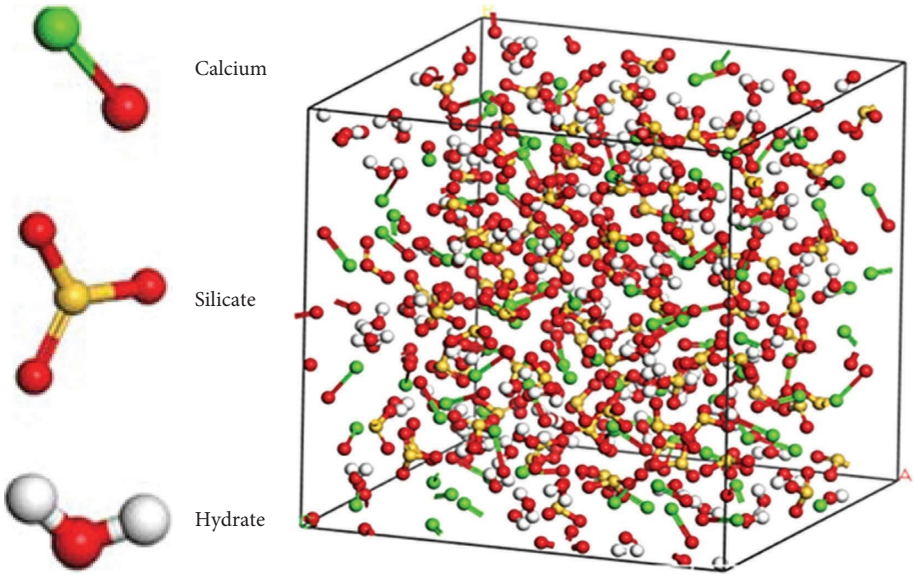

Figure 4: Amorphous cell with CSH cell. (a) Details of CSH. (b) CSH cell structure with ball and stick display.

Table 2: Cell specifications of different types of composite models.

Lattice parameters	a	b	c	Bond length	Length of SWNCT	Percentage of CSH	Percentage of CNT
CSH-CNT-1	40	40	40	1.42	40	99.75	0.25
CSH-CNT-2	40	40	40	1.42	40	99.50	0.5
CSH-CNT-3	40	40	40	1.42	40	99.25	0.75
CSH-CNT-4	40	40	40	1.42	40	99.00	1.00
CSH-CNT-5	40	40	40	1.42	40	99.75	1.25

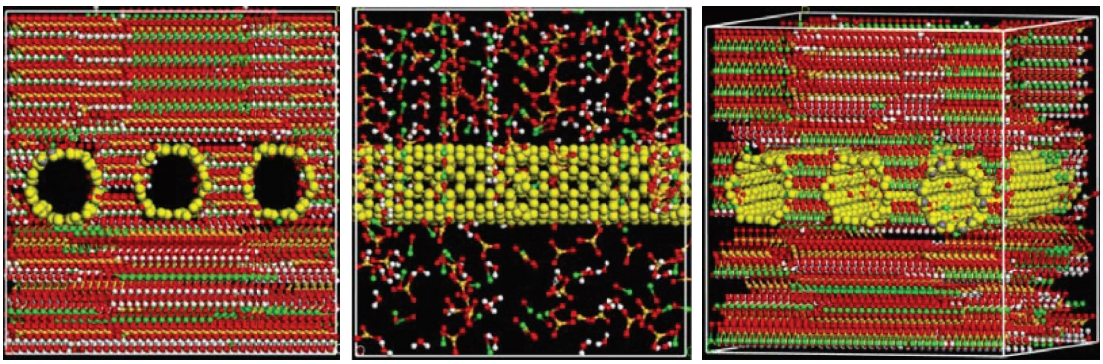

Figure 5: Calcium silicate hydrate reinforced with carbon nanotube model in amorphous cell.

$$E_{\text{total}} = E_b + E_\theta + E_\varphi + E_x + E_{b,b'} + E_{b,\theta} + E_{b,\varphi} + E_{\theta,\varphi} + E_{\theta,\theta'} + E_{\theta,\theta',\varphi} + E_q + E_{vdw}. \quad (2)$$

3.3. Results and Discussion. The results of the MD analysis using the FORCITE module indicate that the energy (kcal/mol) of the system (composite) is reduced, which is a major requirement for further calculating mechanical properties. Figure 6 describes the geometry optimization result to obtain a stable structure or polymorph. So, the atom coordinates and possibly cell parameters are adjusted in an iterative process to minimize the total energy. Optimization of geometry in FORCITE module is based on reducing the magnitude of calculated forces and

stresses until they are smaller than specified convergence. A stress tensor can also be specified to model the system's behaviour under tension, compression, shear, and other conditions. In these cases, the internal stress tensor is increased iteratively until it equals the imposed external stress. Figure 6 demonstrates the geometry optimization of the CSH-CNT composite [28] which has been optimized for the energy and the forces between the bonds are neutralized. The initial temperature observed is 252 K; however, as time progressed, the temperature varied about 170 K on a tiny scale, while the NPT calculation process steadily converged to show that equilibrium has been attained in the system dynamics simulation as shown in Figure 7. Figure 8 indicates that the forces between the bonds have been neutralized and achieved density was approximately 1.67 g/cc. According to the geometry optimization results, the geometry of the CSH-CNT composite has been optimized for energy. A stress tensor is specified to simulate the behaviour of the system under tension, compression, shear, and other conditions to evaluate the mechanical properties.

3.3.1. Mechanical Properties. After geometrical optimization of composite, mechanical properties are calculated using the FORCITE module by performing molecular dynamic analysis. A constant strain value of 0.003 is applied to obtain the mechanical properties such as young's modulus, bulk modulus, shear modulus, and Poisson's ratio of the composites. When carbon nanotube nanoparticles are put in a cement matrix, they effectively bridge fissures in the cement matrix. From Figure 9, average young's modulus has plateaued which indicates that CNT efficiently resists the applied strain. The CSH-CNT composite develops a crack at the end of trial −2, indicating that the model has attained ultimate stress for the strain applied. Attractive electrostatic forces and silicate bonds influence CSH-CNT composite strength, and silicate chain breaking is the primary reason for reduced Young's modulus after trail 2 mixes of the CSH structure due to less O-Si-O bonding [29, 30].

The molecular simulation findings confirm that the CNT embedment improves the mechanical characteristics of CSH. The tensile strength of the CSH-CNT has significantly improved along the direction of the CNTs. From Table 3, it is observed that the CSH-CNT-2 model with 0.50% CNT proportion has the maximum value of Young's modulus in the z-direction, i.e., along the composite's longitudinal axis (perpendicular to the silicate layer). MD analysis yielded Young's modulus of 52.75 GPa for the CSH-CNT-2 composite. As a result, the CNT nucleation process due to rearrangement with CSH gel could eventually develop in the early hydration phase during the formation of composite, which is one explanation for the improvement in mechanical strength of the composite. The CNT's nucleation effect in the composite by measuring the Ca $(OH)_2$ decrement during the hydration process of the CNT containing cement paste is the second reason for the enhancement of mechanical strength [31, 32].

3.3.2. Linking Effect. The "Linking effect" of CNTs in the cement matrix is considered another mechanism for strength enhancement, which could increase the mechanical properties of CSH because they can link the micro and nano cracks in the CSH as shown in Figure 8; thus, it can be referred to as "Linking material." The mechanical properties of a composite are greatly influenced by the cell dimension, the bond length of the CNT, the angle of twist, the type of forcefield, and the lattice system. The covalent linkage between the carbon atoms and SP2 hybridization in the CNTs gives links to all of the microcracks formed, which improves the mechanical strength of the composite. Figure 10 describes the fracture process of each composite system. The crack propagation begun from adjacent sides of SWCNT along fracture line of C-S-H gel, and stress distribution occurs on fracture line of CSH gel and CNT as they embedded inside of the matrix due their adhesion [33, 34]. Henceforth, different failure modes are seen for varying concentration SWCNT. As SWCNT concentration increases, the SWCNT becomes predominately responsible to hold the interlayer atoms of calcium, silicon, and hydrogen forming the "Sandwich structure" of C-S-H gel. This phenomenon causes increase of stress distribution along z direction between CNT and CSH gel and causes cohesive failure [35]. MD simulations illustrate that after achieving cohesive failure, the increase in SWCNT concentration does not help in increase in the fracture strength due to the agglomeration of SWCNT as indicated in microstructural analysis.

3.3.3. Electrical Conductivity. The CASTEP module is based on a quantum mechanics which allows exploring the different properties of CSH-reinforced-CNT composite. To measure the electrical conductivity of the cement nanocomposite, the CASTEP module is used to get the energy band and density of states. Energy band is a distance between an electron's valence band and its conduction band. An electron must be excited to a state in the conduction band at a minimum amount of energy before it can conduct. An energy gap between the lower energy level of the valence band and the higher energy level of the conduction band is required for electrons to become free.

Figure 11 indicates energy band gap for different compositions. Density of states is the number of electrons in materials which allows energy states per unit volume per unit energy state. The size of the bandgap makes the materials exhibit some of their distinct properties. The carbon nanotubes linking effect with the cement matrix increases with more and more addition of CNTs due to which free electrons movement will be obstructed for the transfer of the charges. The cement matrix surrounding the carbon nanotube does not conduct much in comparison to CNTs. The energy gap is more due to which electron excitation is less chance. The electrons will be in a specific energy state depending on the electrical structure around them. The higher energy electrons begin to jump over to the other nanotube as the two nanotubes come closer due to the impact of the electric field [36, 37]. The concentration of

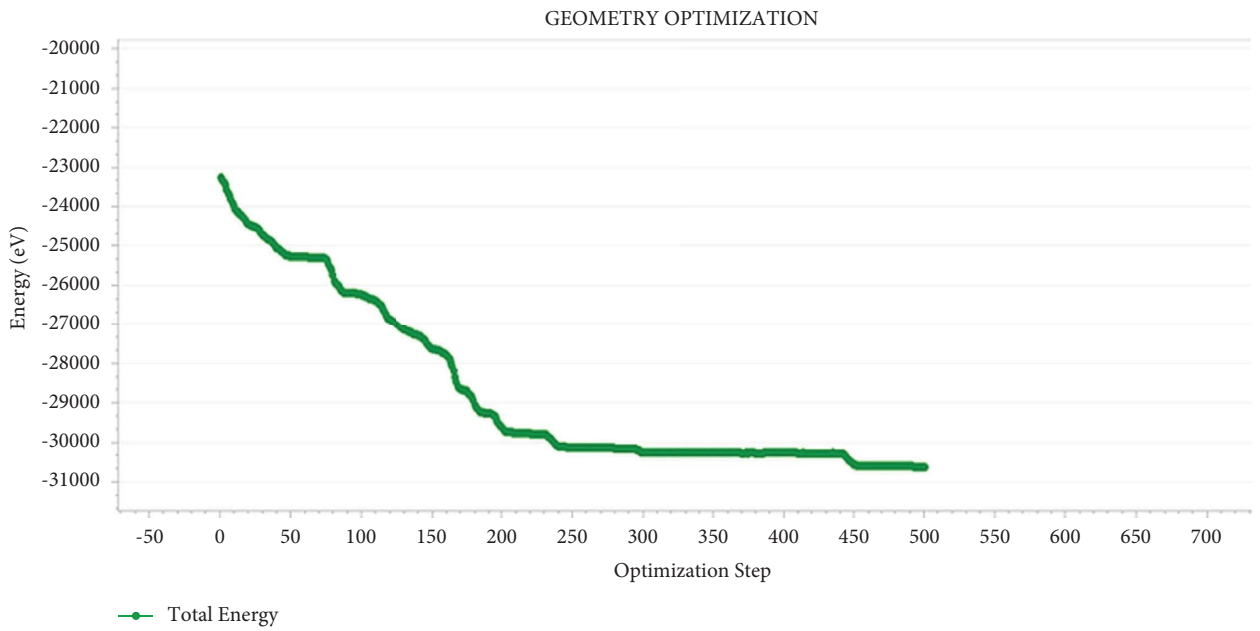

Figure 6: Geometry optimization of cement nanocomposite using FORCITE module.

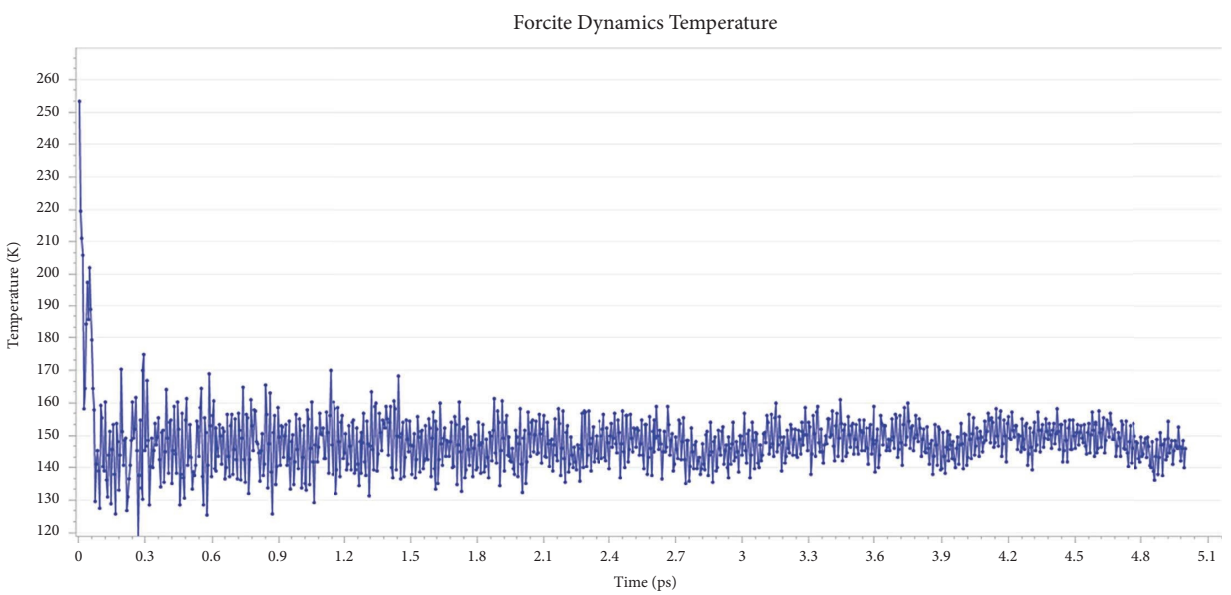

Figure 7: Dynamics temperature of cement nanocomposite using FORCITE module.

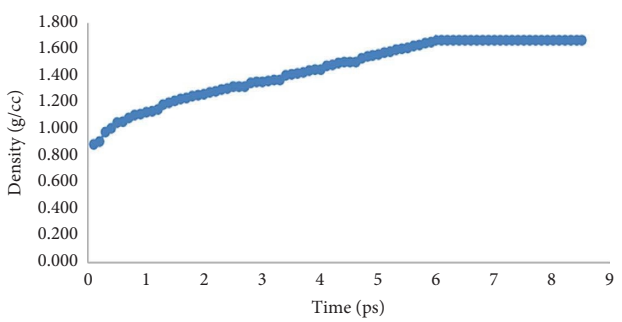

Figure 8: Density (g/cc) vs. time (ps).

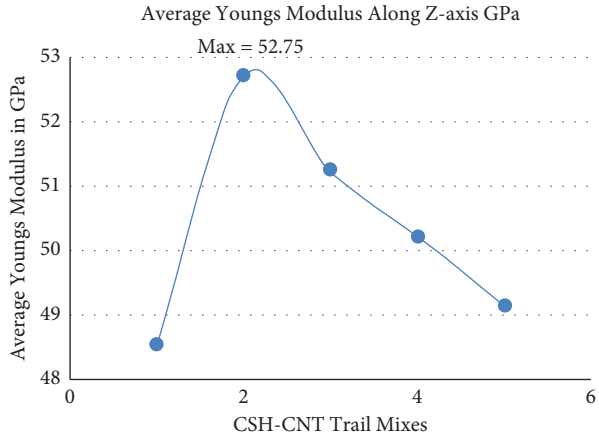

Figure 9: Plot of average Young's modulus along with Z-axis vs. CSH-CNT trail mixes.

Table 3: Calcium silicate hydrate reinforced with carbon nanotube model in amorphous cell.

Composite	Young's modulus in GPa				Shear modulus in GPa				Bulk modulus in GPa				Poisson's ratio			
	E_x	E_y	E_z	E_{avg}	G_{xy}	G_{xy}	G_{zx}	G_{avg}	K_{xy}	K_{yz}	K_{zx}	K_{avg}	μ_{xy}	μ_{yz}	μ_{zx}	μ_{avg}
CSH-CNT-1	31.83	43.87	48.56	41.42	35.57	15.62	32.61	27.93	20.40	28.12	38.54	29.02	0.24	0.24	0.29	0.26
CSH-CNT-2	33.85	48.56	52.75	45.05	38.441	18.53	36.75	31.23	24.53	31.13	41.87	32.51	0.27	0.24	0.29	0.27
CSH-CNT-3	33.12	47.52	51.26	43.97	37.52	15.76	34.86	29.02	23.00	29.33	38.83	30.39	0.26	0.23	0.28	0.26
CSH-CNT-4	32.45	46.52	50.23	43.07	36.12	12.56	32.85	27.18	19.32	28.72	30.53	26.19	0.22	0.23	0.25	0.23
CSH-CNT-5	31.23	45.82	49.15	42.07	35.52	12.23	31.53	26.43	18.59	28.28	29.53	25.47	0.22	0.23	0.24	0.23

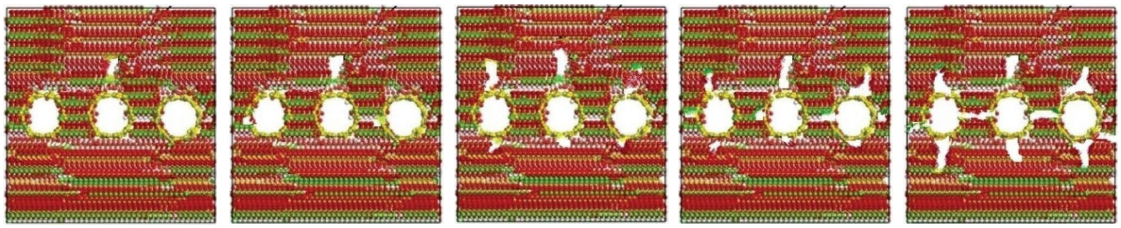

Figure 10: Linking effect of CSH-CNT composite.

CNT in matrix plays a key role in determining the probability of electrons hopping and thus affecting the tunnelling (or electron hopping) resistance. The higher concentration of CNT stimulates the electron hopping to the neighbouring nanotube. The stress distribution at the fracture line between CSH and CNT causes decreases in separation distance of electrons, hence become capable of jumping across the two nanotubes forming a higher current density path in between the nanotubes. In composites with tiny volumes, the curved nanotubes tend to make more connections among themselves, resulting in greater electrical conductivity and a quicker reach of the electrical percolation. Hence, there is a threshold for electrical percolation, above which a stable and continuous flow of electricity has been achieved and a path of conductivity was created between the CSH and CNTs.

The molecular study demonstrates the influence of various factors on the resistance of the nanocomposite, which is primarily dependent on the intertube tunnelling resistance, including the height of barrier potential, CNT length, degree of orientation, and cutoff distance. The homogeneous distribution of short aligned CNTs is found to increase the reinforced nanocomposite's sensitivity to strain [37, 38]. Due to the rapidly availability of the electrons hopping in this tube-like configuration, CNTs exhibit a considerable electrical characteristic based on the atomic configurations. Since there are free electrons in carbon nanotubes, the atomic configurations have a significant effect on their electrical properties [39]. With a gradual increase in the percentage of the carbon nanotubes inclusion in the cement matrix, the conductivity of the system goes on increasing up to 0.5 S/cm, and further the conductivity does

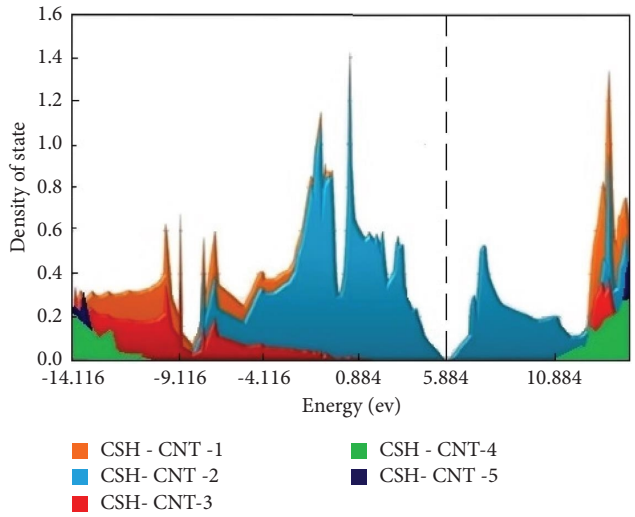

Figure 11: Projected density of states.

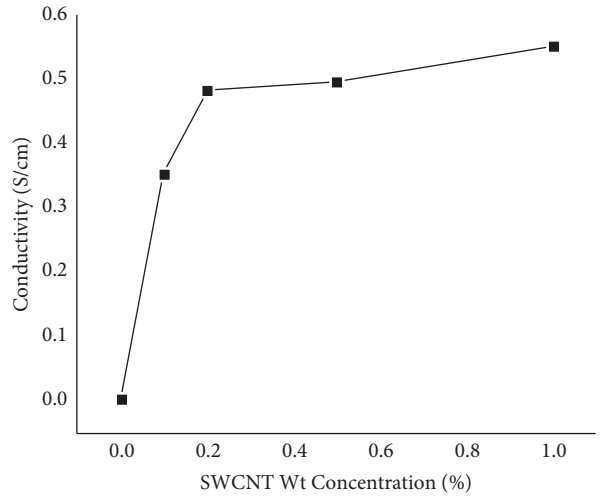

Figure 12: Plot of conductivity vs. percentage of CNT weight fraction.

not increase much as per the increase in CNTs percentage as per Figure 12. Hence, threshold for electrical percolation is observed at 0.5% SWVNT concentration which allows stable and continuous flow of electricity leading conductivity path between the CSH and CNTs.

3.4. Comparative Study. The MD simulation and experimental investigation describe the behaviour of CNT into cement composites. The uniform orientation and non-straight shape of CNTs as well as interfacial bonding need to be taken into consideration in the study as they are well-dispersed within the matrix to produce an isotropic cementitious nanocomposite. CNT-cement nanocomposites in the interfacial area and with CNT waviness revealed extremely high agreement with experimental results. Figure 13 describes the comparison of Young's modulus obtained from the experimental and analytical approach for the various concentrations of CNT cement composites. It is seen that 0.5% of CNT cement composite gives the highest Young's modulus due to well dispersion of CNT as per Figure 3. The error obtained from both the approach is approximately 20% as in analytical study dispersion of CNT is considered to be uniform in the matrix.

4. Representative Volume Element (RVE) Modelling

When a structure is made up of more than one element, it becomes essential to understand its behaviour to assess its properties under the external forces. Representative volume element (RVE) modelling is the most important technique that is used to analyze the smaller scale (micro or nano) materials, mechanical properties, and surface interactions of composite. The RVE is a mathematical model used to calculate the effective characteristics of the homogenised macroscopic composite. In a proposed work, the RVE model is carried out for cement nanocomposite to calculate the effective material constants that are related to stress and strain components such as E, G, and Poisson's ratio. In the proposed work, RVE is made up of transversely isotropic like cement matrix and orthotropic material single-walled carbon nanotube (SWNCT). A homogenized elastic model of square-shaped RVE is considered of length L and cross-sectional area $2a \times 2a$ subjected to external load. The physical dimensions and attributes of the RVE model are presented in Figure 14 and Table 4. When CNTs are equally scattered in concrete structural parts, this model represents the nano-level organization of CNTs. Representative volume element is the technique to calculate the elastic constants. Continuum modelling of continuum mechanics is used to study the RVE modelling using "ANSYS mechanical APDL" (ANSYS Parametric Design Language). Elements like SOLID 65, SOLID 45 commands are used to model CNT and cement matrix [40] and TARGET 170 and CONTACT 174 to define the contact between two surfaces. Similarly for electrical analysis, SOLID 185 for cement matrix and SOLID 227 for CNT is used.

4.1. The Behaviour of CNT Cement Matrix under External Loading. In the present study, gradual increasing of uniformly distributed external loading is applied on cement nanocomposite till failure of composite. This analysis describes the behaviour of CNT onto cement matrix under external load as well as the interface changes between them. Figure 15 shows the distribution of maximum principal stress of composite subjected to a uniform loading "p." It is observed that the end of the CNT projected out from the matrix indicates the pull-out effect due to the application of load. The maximum principal stress value is found to be 17.65 nN/nm^2. The application of load causes CNT to lengthen and expand beyond the cement matrix, which is known as the pull-out effect. The failure of the composite considered at the load of 1 nN/nm as variation of stress is not observed beyond this point as shown in Figure 16.

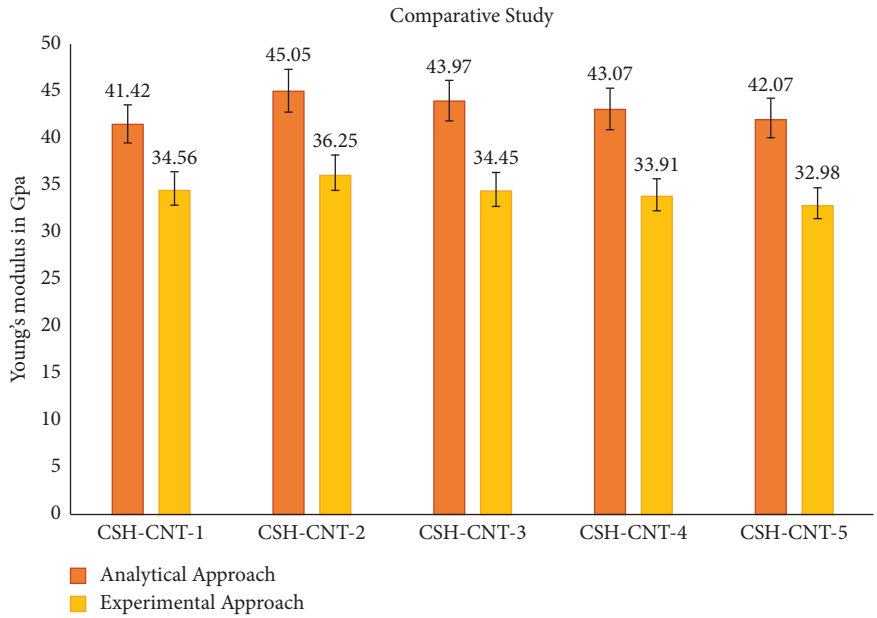

Figure 13: Young's modulus of CNT cement composite obtained from different approaches.

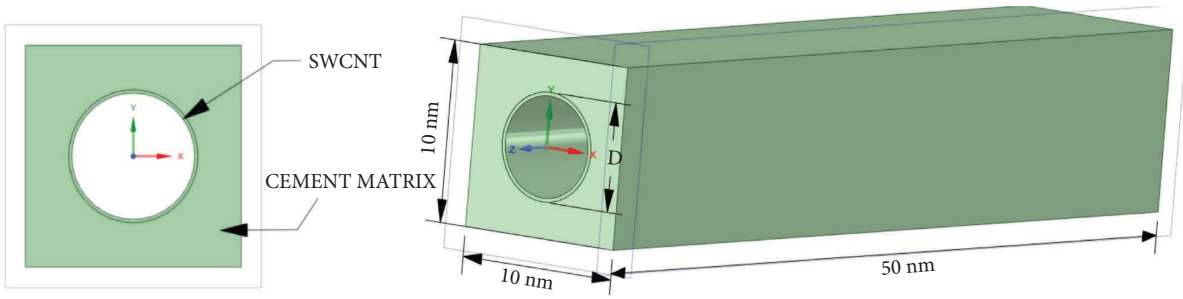

Figure 14: Display of the RVE model with dimensions.

Table 4: Physical dimensions and properties of the RVE model.

Length of CNT, L	50 nm
Outer volume	Cuboidal cement matrix
Inner volume	Hollow cylindrical-shaped SWCNT
Size of RVE model	$10 \times 10 \times 50$ nm
Width and height of cement matrix, 2a	10 nm
Type of RVE model	Square
Volume fractions of CNT	0.45%, 0.89%, 1.34%, 1.78%, and 2.22% of volume of cement matrix
Diameter, D	Diameter varies according to the volume fraction of CNT
Density of CNT	$1.34e^{-24}$ kg/nm^3
Density of cement matrix	$2400e^{-9}$ kg/nm^3
Young's modulus of CNT	1000 GPa
Young's modulus of cement matrix	5, 20, 100, 200 Nn/nm^2
Poisson's ratio of CNT	0.2
Poisson's ratio of cement matrix	0.3
Electrical resistivity of CNT	10^5 ohm·nm
Isotropic resistivity	5.5×10^{12} ohm·nm

Figure 17 shows the maximum deflection at the centre of the bottom fibres of CNT cement composite due to consistent loading. At the failure load of 1 nN/nm, no deflection or displacement is found nearer to the support, while the maximum deflection is found to be 0.61899 nm at centre. Figure 18 explains the relationship between load and deflection. The uniform deflection is observed up to the load of 0.4 nN/nm; after this, gradual increase of deflection takes place until the load of 1 nN/nm, at which the deflection tends to be maximal.

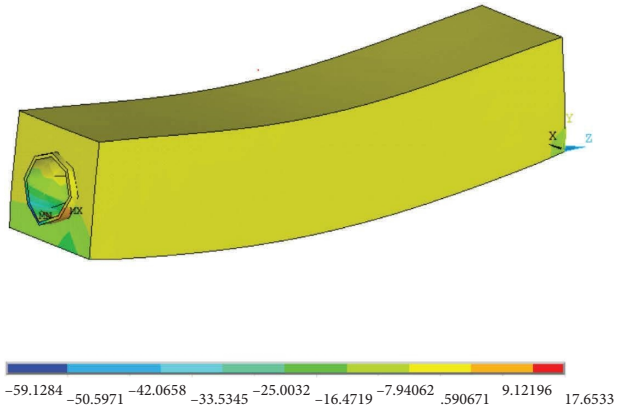

Figure 15: Distribution values of maximum principal.

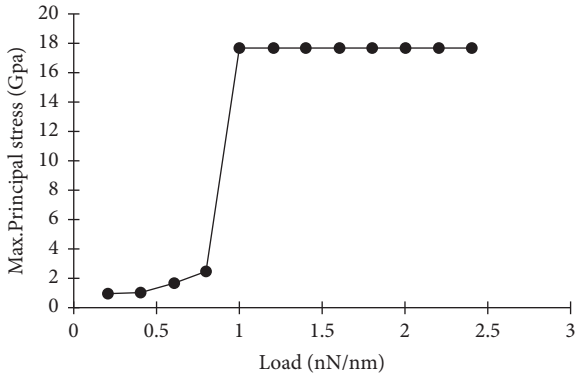

Figure 16: Pressure vs. max. principal stress through CNT-cement composite.

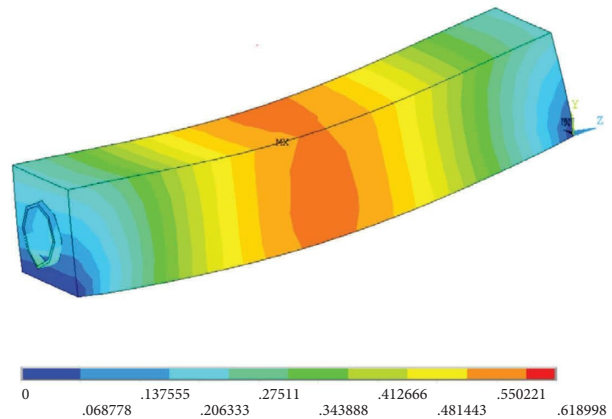

Figure 17: Maximum deflection in CNT-cement composite.

4.2. Mechanical Properties of RVE Modelling. The previous RVE model is examined for initial uniform loading of 0.2 nN/nm to obtain the elastic constants in the z-direction considering the CNT pull-out effect and axial elongation. Deformations in the x and y directions are also considered to calculate the elastic constants in the x and y directions, respectively. The following constants were computed by

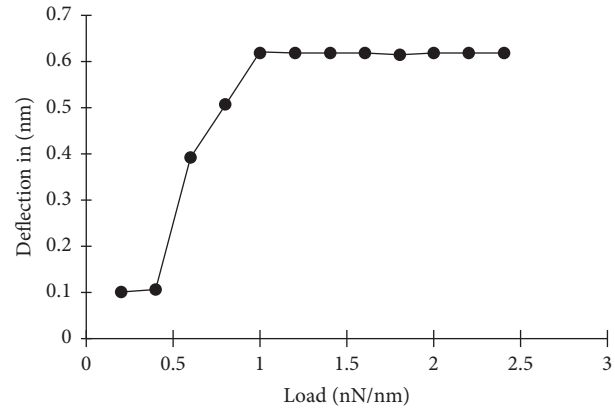

Figure 18: Relation between the load applied and deflection.

inputting the results of the ANSYS analysis into the following mentioned formulas [41].

4.2.1. Expression to Determine E_z

$$E_z = \frac{\sigma_1}{\varepsilon_z}, \tag{3}$$

where $\varepsilon_z = \Delta L/L$ = axial strain in z direction, σ_1 = effective normal stress in z-direction, and E_z = effective Young's modulus in z-direction

4.2.2. Expression to Determine E_x and v_{xy}

$$E_x = E_y = \frac{1}{(\Delta y/pa) + \left(v_{zx}^2/Ez\right)},$$
$$v_{xy} = -\frac{\left((\Delta x/pa) + \left(v_{zx}^2/Ez\right)\right)}{\left((\Delta y/pa) + \left(v_{zx}^2/Ez\right)\right)}, \tag{4}$$

where v_{zx} = effective Poisson's ratio; p = magnitude of uniform loading; a = half of the width of the RVE; E_x, E_y = effective Young's modulus in x, y-direction; E_z = effective Young's modulus in the z-direction; Δx = change in dimension in the x-direction; and Δy = change in dimension in the y-direction.

4.2.3. Expression for Calculating the Modulus of Rigidity

$$G = \frac{E}{2(1+v)}, \tag{5}$$

where G = modulus of rigidity; E = effective Young's modulus; and v = effective Poisson's ratio

4.2.4. Formula to Convert Weight to Volume Fraction

$$f = \frac{\text{fw}}{\text{fw} + (1 - \text{fw})(\rho f/\rho \text{m})}, \tag{6}$$

where f = volume fraction of CNT fibre in %, fw = weight fraction of fibre, ρf = density of CNT fibre in gm/cm^3, and ρm = density of cement matrix in gm/cm^3

εx, εz, σz, Δx, and Δy are extracted from the results generated after completing the analysis in ANSYS APDL. These values are substituted further in the expressions (5, 6, and 7) to obtain the values of elastic constant for composite as presented in Table 5.

From Table 5, it is observed that elastic constants are found to be higher for the 0.89 percent volume fraction of CNT which appears to be the optimum value of CNT, as shown visually in Figure 17. The stiffness in all three directions increases with the increasing of Young's modulus. The pull out of CNT seen in the z-direction leads to the increase of stress at the interface due to the effective load transfer from the cement matrix. This improves the stiffness in the z-direction. The relationship between nanocomposite longitudinal modulus Ez/Em and matrix modulus is presented in Figure 17. It indicates that when the matrix modulus increases, the stiffness also increases which improves the strength of composite [42]. Another key factor to remember is that the larger difference between constituent moduli leads to the improvement of the effective modulus of the nanocomposite [43]. Also, Figure19 shows that for all volume fractions, Ez/Em is less than unity, indicating that nanotubes do not contribute to the strength in the z-direction [44]. However, the Ez/Em value of 0.89 percent is the highest when compared to other volume fractions for all matrix modulus, especially for the matrix modulus of 50 and 200.

4.3. Electrical Analysis of RVE Model under Mechanical Loading. RVE analysis is a popular technique for micromechanical modelling of heterogeneous materials. It can be used to perform a homogenization analysis to obtain effective properties, as well as a dehomogenization analysis to obtain the material's local fields and failure. Its popularity can be attributed primarily to the maturity and acceptance of commercial finite element software. As long as the Hill–Mandel macrohomogeneity condition is satisfied, various boundary conditions (BCs) can be used for the RVE analysis. Kinematically uniform BCs (KUBCs), statically uniform BCs (SUBCs), and periodic BCs are the three most common types of BCs (PBCs). Both KUBCs and SUBCs are relatively simple to apply for. PBCs can be used in conjunction with coupled equation constraints.

Here, the voltage of 20 V was maintained constant till the end of the analysis. The model is analyzed for mechanical loading, and variation in current density with respect to change in magnitude of load is noted down, and resistance is calculated for respective values as presented in Table 6. Figure 20 depicts the distribution of the current density due to the applied load and voltage. Since the carbon is a conductor of electricity, therefore, the distribution of current density is uniform across the CNT [45, 46]. The maximum value of current density is stated in terms of nA/nm^2. The end points of the CNT have the lowest current density. When varied magnitudes of external pressure were applied to CNT, changes in current density were observed as shown in Figure 21. Ohm's equation is used to calculate the resistance at a given amount of load. From Figure 22, it is seen that the resistance is found to be high for the initial loading of 0.2 nN/nm, with a value of 1.83486×10^{-16} ohm·nm. However, as the loading increases, the resistance decreases, making the material more conductive for additional increases in load. This is due to, when a load is applied to CNT, the pull-out occurred which increases the strain. Pull out in the z-direction exhibits no change in the cross-section area, implying that the surface area is growing. Increased surface area leads to increased conductivity and, as a result, less resistance. The effective conductivity in the axial direction, i.e., normal to the plane of the nanoscale RVE, is calculated by averaging of the local conductivities of the nanoscale RVE, assuming that the electron hopping pathways extend through the length of infinitely long CNTs [46–48].

5. Interaction between CNT and Cement Matrix

5.1. Contact Penetration. When the external pressure is applied to the CNT cement composite, the CNT expands in the z-direction. Therefore, CNT in the cement matrix provides the support and stability from internal surface to the composite. As a result of the strain and change in the length of the CNT tube, the CNT attempts to penetrate the cement matrix causing tension between the two surfaces as shown in Figure 23 [49, 50]. The penetration is measured in terms of stress. The greater the tension indicates the greater the penetration. Figure 24 shows the increase of stress due to the increase of external load leading to the uniform increase in strain. The pull out of CNT signifies increased penetration of CNT which leads to an increase in the value of stress [51, 52].

5.2. Contact Sliding. Due to the external applied pressure on composite cause sliding of CNT from cement matrix along with pull out effect, the CNT slid from its centre section along the inner surface across cement matrix. This is due to CNT's outer surface movement, and penetration of the CNT into the cement matrix is restricted due to the action sliding as depicted as shown in Figures 25–27. The largest sliding occurs at the support, and sliding is comparably less at the centre resulting in lower magnitudes of stresses in that location. Figure 28 shows that the load increases cause the sliding, which increases the stress in composite. It is observed that cement composite fails at 1 nN/nm^2, because the increasing of sliding is maximum at that load. With further increase of load, the stress value remains constant, indicating that there is no additional sliding. The maximum stress obtained is found to be 0.1733 nN/m^2 at a load of 1 nN/nm.

5.3. Contact Pressure. The deformation of the composite was observed due to the application of pressure, but it was assumed that the deformation of the CNT inside the cement matrix would apply some internal pressure on the inner area of the cement matrix [53, 54]. According to Figure 29, the largest amount of stress is observed at the bottom tip of the CNT near the support. Figure 30 depicts the relationship between pressure and the stress caused by contact pressure. Stress due to load exerted by CNT over cement matrix

Table 5: Mechanical properties of nanocomposite w.r.t the volume fraction of CNT.

Composite	Wt. fraction (%)	Vol. fraction (%)	Young's modulus in GPa				Poisson's ratio				Shear modulus in GPa			
			E_x	E_y	E_z	E_{avg}	μ_{xy}	μ_{yz}	μ_{zx}	μ_{avg}	G_{xy}	G_{xy}	G_{zx}	G_{avg}
CSH-CNT-1	0.25	0.45	38.64	38.64	51.85	40.04	0.23	0.23	0.27	0.24	15.70	15.7	20.14	12.27
CSH-CNT-2	0.5	0.89	44.89	44.89	57.22	49.00	0.27	0.27	0.31	0.28	17.50	17.50	59.84	31.61
CSH-CNT-3	0.75	1.34	43.66	43.66	54.67	47.33	0.26	0.26	0.29	0.27	17.13	17.13	21.18	18.48
CSH-CNT-4	1	1.78	41.72	41.72	53.48	45.64	0.25	0.25	0.26	0.25	16.63	16.63	21.22	18.16
CSH-CNT-5	1.25	2.22	40.18	40.18	52.38	44.24	0.23	0.23	0.24	0.23	16.63	16.63	21.12	18.12

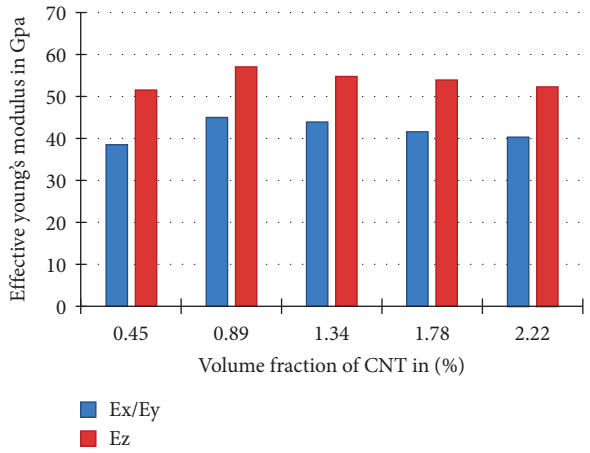

Figure 19: Volume vs effective young's modulus.

Table 6: Values of current density and resistance w.r.t loads.

Load (nN/nm)	Current density (nA/nm^2)	Resistance (Ω·nm)
0.2	$0.109E+18$	$1.83486E-16$
0.4	$0.128E+18$	$1.5625E-16$
0.6	$0.176E+18$	$1.13636E-16$
0.8	$0.234E+18$	$8.54701E-17$
1.0	$0.294E+18$	$6.7567E-17$
1.2	$0.370E+17$	$5.40541E-17$

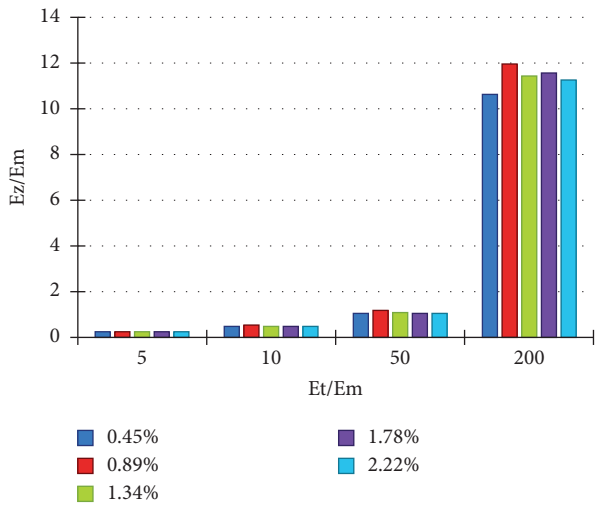

Figure 20: Longitudinal modulus vs matrix modulus.

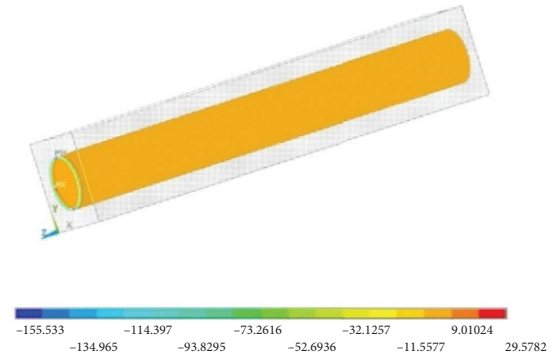

Figure 21: Distribution of current density in CNT.

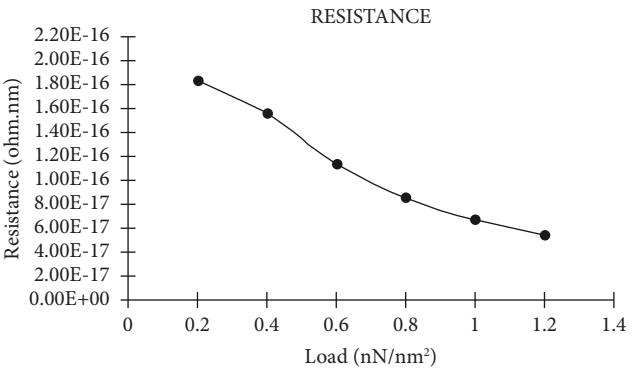

Figure 22: Load vs. resistance.

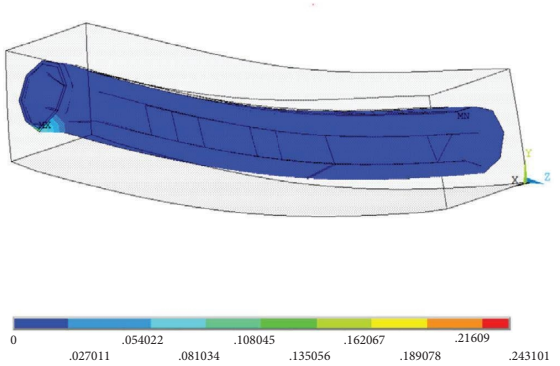

Figure 23: Effect of penetration of CNT into cement matrix.

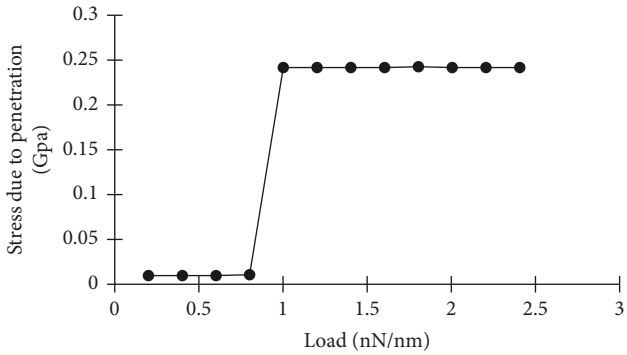

Figure 24: Contact penetration.

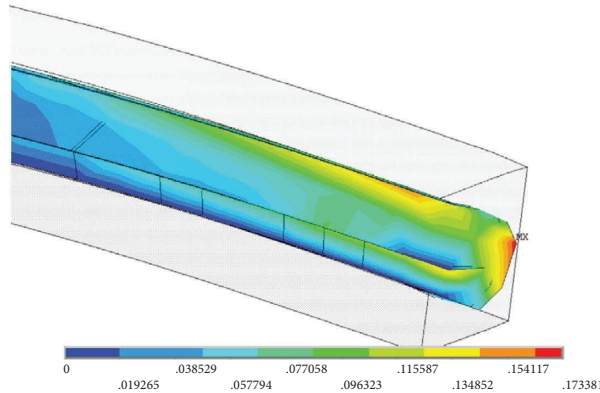

Figure 27: Reduction in stresses from support to centre.

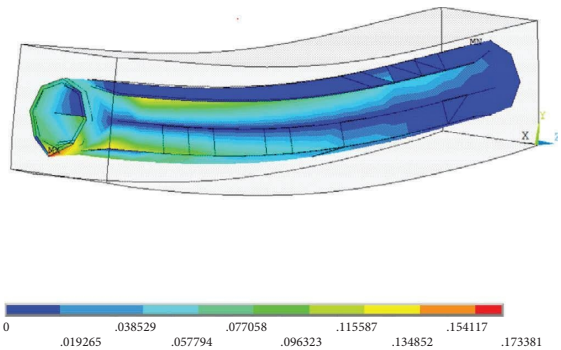

Figure 25: Sliding of CNT through the cement matrix.

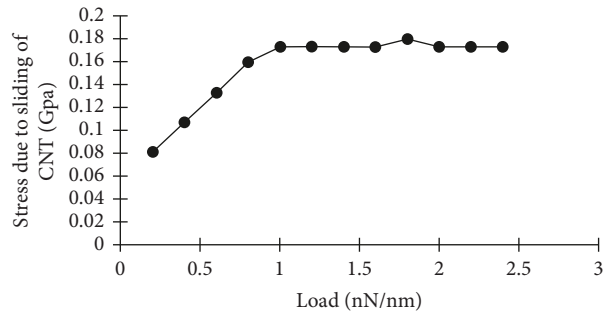

Figure 28: Representation of stress with an increase in pressure.

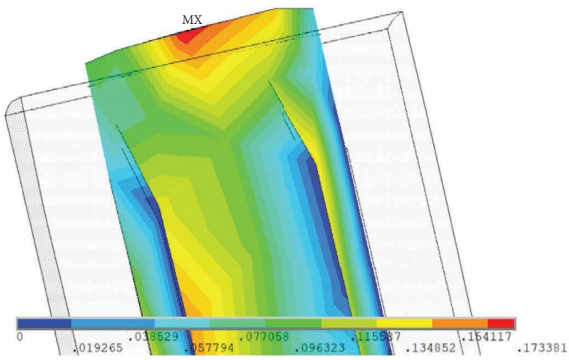

Figure 26: CNT pulled out at support due to sliding due to the application of pressure.

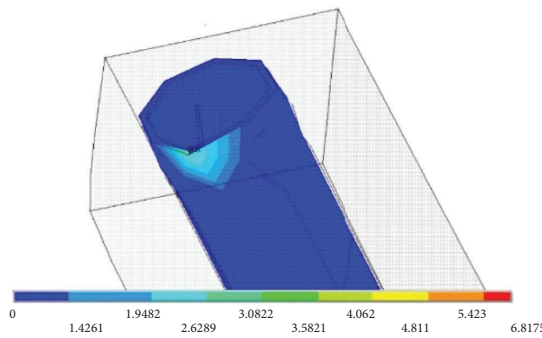

Figure 29: Magnified image of exact location for the maximum value of stress.

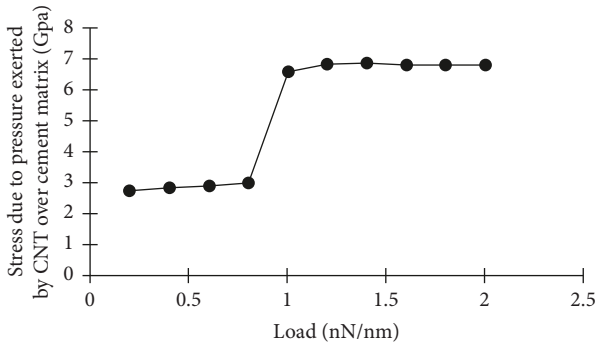

Figure 30: Relation between pressure location of applied and stress-induced due to contact pressure.

slightly increases up to 0.8 nN/nm; at 1 nN/nm, the stress increases to the maximum value of 6.8175 nN/nm, and for further increase in pressure, the stress is constant, and at load of 1 nN/nm, the maximum pull out is achieved.

6. Conclusion

From the previous studies, it has been revealed that concentration of CNT into matrix plays crucial role on interfacial interaction between them which significantly influence on mechanical and electrical properties. The molecular dynamic study proves to be an effective method to compute the elastic constant of composite. From the molecular dynamic analysis and experimental results, it is evident that the inclusion of carbon nanotube in the cement matrix enhances the mechanical properties of the composite. The weight fraction and volume fraction of CNT in the cement matrix and dispersion of CNTs in the cement matrix play major role in the mechanical and electrical properties. The molecular dynamic simulation inculcates the "linking-effect" of CNTs with the CSH gel which can effectively act as a filler material. The density of the CSH-CNT-2 composite is found using the FORCITE module which is 1.67 g/cc. The optimum dosage of CNT is obtained at a 0.50% weight fraction and 0.89% volume fraction of CNT in the cement matrix which yields the better properties. The covalent bond between the carbon atoms and SP^2 hybridization in the CNTs has proved that CNTs have good longitudinal resistance and provide the linking to all the microcracks generated which in turn enhances the mechanical strength of the composite.

From the RVE modelling, it can be observed that the effective load transfer of CNTs is due to the availability of larger surface area, which increases in mechanical properties. From the interfacial interaction of CNT and cement matrix, it is observed that increase in stiffness is due to the sliding of CNT causing pull-out effect which provides the effective load transfer through CNT over cement matrix. However, more increase in CNT weight and volume fraction causes a reduction in mechanical properties due to the agglomeration of nanotubes as observed from the SEM analysis.

The electrical conductivity of the composite at 0.50% of the CNT fraction is found to be 0.56 s/cm stipulating as increasing of weight percentage of CNTs in cement matrix enhances the mobility of electrons. With further increase in CNT fraction, it is observed that conductivity tends to attain saturation due to agglomeration of electrons, charge imbalance, and hopping of electrons into the core of CNT which decrease the resistance. In RVE analysis, constant voltage with the increase in the mechanical loading demonstrates the increase of conductivity due to increases in the surface area resulting in a reduction of resistance. After the failure of composite, the value of resistance and conductivity becomes constant. Hence, from previous studies, it is concluded that nanocement composites are promising smart materials in present which possess greater load carrying capacity, mechanical properties, and electrical properties and can be used for real time applications.

Data Availability

Data are available upon request.

Conflicts of Interest

The authors declare that they have no conflicts of interest.

Acknowledgments

The authors extend their appreciation to the Deanship of Scientific Research at King Khalid University, Saudi Arabia, for funding this work through the large research groups program under grant number R.G.P 2/76/44.

References

[1] S. Parveen, S. Rana, and R. Fangueiro, "A review on nanomaterial dispersion, microstructure and mechanical properties of carbon nanotube and nanofiber reinforced cementitious composites," *Journal of Nanomaterials*, vol. 2013, Article ID 710175, 19 pages, 2013.

[2] B. S. Sindu and S. Sasmal, "Properties of carbon nanotube reinforced cement composite synthesized using different types of surfactants," *Construction and Building Materials*, vol. 155, pp. 389–399, 2017.

[3] X. Wu and L. Dai, "Carbon nano-tubes in improving the mechanical property of cement-based composite materials," *Frattura Ed Integrità Strutturale*, vol. 11, no. 41, pp. 388–395, 2017.

[4] A. Rahim and S. R. Nair, "Influence of nano-materials in high strength concrete," *Journal of Chemical and Pharmaceutical Sciences*, vol. 974, 2016.

[5] A. M. Hunashyal, G. V. Sundeep, S. S. Quadri, and N. R. Banapurmath, "Experimental investigations to study the effect of carbon nanotubes reinforced in cement-based matrix composite beams," *Proceedings of the Institution of Mechanical Engineers-Part N: Journal of Nanoengineering and Nanosystems*, vol. 225, no. 1, pp. 17–22, 2011.

[6] E. E. Gdoutos, M. S. Konsta-Gdoutos, P. A. Danoglidis, and S. P. Shah, "Advanced cement based nanocomposites reinforced with MWCNTs and CNFs," *Frontiers of Structural and Civil Engineering*, vol. 10, no. 2, pp. 142–149, 2016.

[7] A. Carriço, J. A. Bogas, A. Hawreen, and M. Guedes, "Durability of multi-walled carbon nanotube reinforced

concrete," *Construction and Building Materials*, vol. 164, pp. 121–133, 2018.

[8] A. M. Rashad, "Effect of carbon nanotubes (cnts) on the properties of traditional cementitious materials," *Construction and Building Materials*, vol. 153, pp. 81–101, 2017.

[9] D. S. Hou, H. Ma, and Z. Li, "Morphology of calcium silicate hydrate (ceseh) gel: a molecular dynamics study," *Advances in Cement Research*, vol. 25, no. 1, p. 1e12, 2013.

[10] H. M. Jennings, "A model for the microstructure of calcium silicate hydrate in cement paste," *Cement and Concrete Research*, vol. 30, no. 1, pp. 101–116, 2000.

[11] H. M. Jennings, "Refinements to colloid model of ceseh in cement: cm II," *Cement and Concrete Research*, vol. 38, no. 3, 2008.

[12] J. S. Dolado, M. Griebel, J. Hamaekers, and F. Heberc, "The nano-branched structure of cementitious calciumesilicatee-hydrate gel," *Journal of Materials Chemistry*, vol. 21, no. 12, p. 445, 2011.

[13] G. Costantinides and F. Ulm, "The effect of two types of ceseh on the elasticity of cement-based materials: result from nanoindentation and micromechanical modeling," *Cement and Concrete Research*, vol. 34, no. 1, p. 67e80, 2004.

[14] R. Shahsavari, M. J. Buechler, R. J. M. Pellenq, and F. J. Ulm, "First-principles study of elastic constants and interlayer interactions of complex hydrated oxides: case study of tobermorite and jennite," *Journal of the American Ceramic Society*, vol. 92, no. 10, 2009.

[15] R. J. M. Pellenq, A. Kushima, R. Shahsavari et al., "A realistic molecular model of cement hydrates," *Proceedings of the National Academy of Sciences of the United States of America*, vol. 106, no. 38, pp. 16102–16107, 2009.

[16] K. Ioannidou, K. J. Krakowiak, M. Bauchy et al., "Mesoscale texture of cement hydrates," *Proceedings of the National Academy of Sciences of the United States of America*, vol. 113, no. 8, pp. 2029–2034, 2016.

[17] K. Grabowski, P. Zbyrad, T. Uhl, W. J. Staszewski, and P. Packo, "Multiscale electro-mechanical modeling of carbon nanotube composites," *Computational Materials Science*, vol. 135, pp. 169–180, 2017.

[18] S. H. Park, H. K. Jang, Y. Park et al., "Prediction of mechanical properties of MWCNT-reinforced composites using the RVE model," *Modern Physics Letters B*, vol. 32, no. 18, Article ID 1850196, 2018.

[19] Z. Ounaies, C. Parkb, K. E. Wiseb, E. J. Siochic, and J. S. Harrison, "Electrical properties of single wall carbon nanotube reinforced polyimide composites," *Composites Science and Technology*, vol. 63, no. 11, pp. 1637–1646, 2003.

[20] J. Norambuena-Contreras, A. Cartes, I. Gonzalez-Torre, M. Chavez, and A. Kanellopoulos, "Effect of metallic waste addition on the physical and mechanical properties of cement-based mortars," *Applied Sciences*, vol. 8, no. 6, p. 929, 2018.

[21] M. Eftekhari and S. Mohammadi, "Molecular dynamics simulation of the nonlinear behavior of the CNT-reinforced calcium silicate hydrate (C-S-H) composite," *Composites Part A: Applied Science and Manufacturing*, vol. 82, pp. A78–A87, 2016.

[22] Y. Zhou, H. Zheng, Y. Qiu, X. Zou, and J. Huang, "A molecular dynamics study on the structure, interfaces, mechanical properties, and mechanisms of a calcium silicate hydrate/2D-silica nanocomposite," *Frontiers in Materials*, vol. 7, p. 127, 2020.

[23] D. Hou and L. Zongjin, "Large-scale simulation of calcium silicate hydrate by molecular dynamics," *Advances in Cement Research*, vol. 27, no. 10, p. 1680, 2014.

[24] W. Wu, A. Al-Ostaz, A. H. D. Cheng et al., "Computation of elastic properties of portland cement using molecular dynamics," *Journal Of Nanomechanics And Micromechanics*, vol. 1, no. 2, pp. 84–90, June 2011.

[25] O. Bernard, F.-J. Ulm, and E. Lemarchand, "A multiscale micromechanics-hydration model for the early-age elastic properties of cement-based materials," *Cement and Concrete Research*, vol. 33, no. 9, pp. 1293–1309, 2003.

[26] C. R. Song, H. Cho, Y.-H. Jung, A. H. D. Cheng, and A. Al-Ostaz, "Bridging molecular, particulate, and continuum mechanics for geomechanics application," *Advances in Measurement and Modeling of Soil Behavior*, pp. 18–21, ASCE, Denver, CO, USA, 2007.

[27] H. Manzano, J. Dolado, and A. Ayuela, "Elastic properties of the main species present in portland cement pastes," *Acta Materialia*, vol. 57, no. 5, pp. 1666–1674, 2009.

[28] M. Eftekhari and S. Mohammadi, "Molecular dynamics simulation of the nonlinear behavior of the CNT-reinforced calcium silicate hydrate (C-S-H) composite," *Composites Part A: Applied Science and Manufacturing*, vol. 82, pp. 78–87, 2016.

[29] S. Sharma, P. Kumar, and R. Chandra, "Mechanical and thermal properties of graphene–carbon nanotube-reinforced metal matrix composites: a molecular dynamics study," *Journal of Composite Materials*, vol. 51, no. 23, pp. 3299–3313, 2017.

[30] S. Sharma, S. Tiwari, S. Shakya, and N. Kumar, "Mechanical Properties and thermal conductivity of pristine and functionalized carbon nanotube reinforced metallic glass composites: a molecular dynamics approach," *Defence Technology*, vol. 17, no. 1, pp. 234–244, 2021.

[31] L. Lee and I. Yahya, "Electrical and structural characterization of graphene carbon nanotubes hybrids structures," *ASM Sc. J*, vol. 12, no. 4, pp. 83–89, 2019.

[32] O. Kharissova, L. Torres-Martínez, and B. Kharisov, "Recent trends of reinforcement of cement with carbon nanotubes and fibers," *Advance in carbon Nanostructures*, vol. 10, pp. 5772–62292, 2016.

[33] S. Sharma, R. Chandra, P. Kumar, and N. Kumar, "Thermo-mechanical characterization of multi-walled carbon nanotube reinforced polycarbonate composites: a molecular dynamics approach," *Comptes Rendus Mecanique*, vol. 343, no. 5-6, pp. 371–396, 2015.

[34] R. Qin, A. Zhou, Z. Yu, Q. Wang, and D. Lau, "Role of carbon nanotube in reinforcing cementitious materials: an experimental and coarse-grained molecular dynamics study," *Cement and Concrete Research*, vol. 147, Article ID 106517, 2021.

[35] S. Bs and S. Sasmal, "Molecular dynamics simulations for evaluation of surfactant compatibility and mechanical characteristics of carbon nanotubes incorporated cementitious composite," *Construction and Building Materials*, vol. 253, Article ID 119190, 2020.

[36] T. Tarighat and D. Tavakoli, "Estimation of the elastic properties of important calcium silicate hydrates in nano-scale-a molecular dynamics approach," *Journal of Rehabilitation in Civil Engineering*, vol. 7, no. 4, pp. 18–36, 2019.

[37] M. K. Hassanzadeh-Aghdam, R. Ansari, M. J. Mahmoodi, A. Darvizeh, and A. Hajati-Modaraei, "A comprehensive study on thermal conductivities of wavy carbon nanotube-reinforced cementitious nanocomposites," *Cement and Concrete Composites*, vol. 90, pp. 108–118, 2018.

[38] M. Haghgoo, R. Ansari, M. K. Hassanzadeh-Aghdam, and M. Nankali, "A novel temperature-dependent percolation model for the electrical conductivity and piezoresistive sensitivity of carbon nanotube-filled nanocomposites," *Acta Materialia*, vol. 230, Article ID 117870, 2022.

[39] J.-Q. Wang, H.-L. Kang, and Y. Zhang, "Simulation calculation and analysis of electronic structure and electrical properties of metal-doped SnO2," *Advances in Materials Science and Engineering*, vol. 2018, Article ID 9086195, pp. 1–10, 2018.

[40] *Materials Studio. User's Manual*, Accelrys, Inc, San Diego, CA, USA, 2015.

[41] X. L. Chen and Y. J. Liu, "Square representative volume elements for evaluating the effective material properties of carbon nanotube-based composites," *Computational Materials Science*, vol. 29, no. 1, pp. 1–11, 2004.

[42] L. Y. Chan and B. Andrawes, "Characterization of the uncertainties in the constitutive behavior of carbon nanotube/cement composites," *Science and Technology of Advanced Materials*, vol. 10, no. 4, Article ID 045007, 2009.

[43] B. S. Sindhu, S. Sasmal, and S. Gopinath, "Numerical simulation of CNT incorporated cement," *International Scholarly and Scientific Research and Innovation*, vol. 6, no. 5, 2012.

[44] Y. J. Liu and X. L. Chen, "Continuum models of carbon nanotube-based composites using the boundary element method," *Electronic Journal of Boundary Elements*, vol. 1, no. 2, pp. 316–335, 2007.

[45] H. M. Seyed, "Effect of carbon nanotube dispersion on the mechanical properties of nanocomposites considering interface effect," *International Journal of Current Research*, vol. 4, no. 8, pp. 4366–4373, 2016.

[46] A. K. Singh, S. Harsha, and A. Parashar, "Finite Element Analysis of CNT reinforced epoxy composite due to Thermo-Mechanical loading," *Procedia Technology*, vol. 23, pp. 138–143, 2016.

[47] P. Yang, S. Chowdhury, and N. Neithalath, "Strain sensing ability of metallic particulate reinforced cementitious composites: experiments and microstructure-guided finite element modeling," *Cement and Concrete Composites*, vol. 90, pp. 225–234, 2018.

[48] A. Abbass, M. C. Paiva, D. V. Oliveira, P. B. Lourenço, and R. Fangueiro, "Graphene/polyurethane nanocomposite coatings–Enhancing the mechanical properties and environmental resistance of natural fibers for masonry retrofitting," *Composites Part A: Applied Science and Manufacturing*, vol. 166, Article ID 107379, 2023.

[49] M. Haghgoo, R. Ansari, S. H. Jang, M. Kazem Hassanzadeh-Aghdam, and M. Nankali, "Developing a high-efficiency predictive model for self-temperature-compensated piezoresistive properties of carbon nanotube/graphene nanoplatelet polymer-based nanocomposites," *Composites Part A: Applied Science and Manufacturing*, vol. 166, Article ID 107380, 2023.

[50] H. Fallahi, O. Kaynan, and A. Asadi, "Insights into the effect of fiber–matrix interphase physiochemical-mechanical properties on delamination resistance and fracture toughness of hybrid composites," *Composites Part A: Applied Science and Manufacturing*, vol. 166, Article ID 107390, 2023.

[51] G. Ongaro, R. Bertani, U. Galvanetto, A. Pontefisso, and M. Zaccariotto, "A multiscale peridynamic framework for modelling mechanical properties of polymer-based nanocomposites," *Engineering Fracture Mechanics*, vol. 274, Article ID 108751, 2022.

[52] Y. J. Liu and X. L. Chen, "Evaluations of the effective material properties of carbon nanotube-based composites using a nanoscale representative volume element," *Mechanics of Materials*, vol. 35, no. 1-2, pp. 69–81, 2003.

[53] M. T. Le and S. C. Huang, "Hexagonal representative volume element for modeling and analysis of mechanical properties of carbon nanotube reinforced composites," *Applied Mechanics and Materials*, vol. 496, no. 500, pp. 251–254, 2014.

[54] Ansys, "ANSYS Mechanical APDL element reference," 2011, http://www.ansys.com/.